International Journal of Multiphase Flow 34 (2008) 869–878

Contents lists available at ScienceDirect

International Journal of Multiphase Flow

journal homepage: www.elsevier.com/locate/ijmulflow

Three-dimensional simulation of a dust lifting process with varying parameters

C.G. Ilea *, P. Kosinski, A.C. Hoffmann

Department of Physics and Technology, The University of Bergen, Allégaten 55, 5007 Bergen, Norway

ARTICLE INFO

Article history:
Received 16 June 2007
Received in revised form 2 December 2007
Available online 17 March 2008

Keywords:
Dust lifting
Fluid mechanics
Mathematical modelling
Multiphase flow
Particle collision

ABSTRACT

This article presents modelling considerations and simulation results for a dust lifting process in a three-dimensional domain. The Eulerian–Lagrangian modelling technique is used. Multiple simulations with different values for the number of particles were performed. The results of the simulations are shown as snapshots of particle position at certain points in time after the passage of a shock wave. Statistical data for the particle positions and collisions are presented. These are: the average height of the particles, the mean square displacement of the particles and the cumulative number of recorded collisions plotted as functions of time. The particle averaged kinetic energy and the mechanical energy lost by particles during collisions are recorded as functions of time in order to study the motion of particles. The results show that simulations of an increasing number of particles render a less intense lifting effect and, more importantly, that the inter-particle and particle–wall collisions represent essential phenomena and need to be included in this type of model. Also, a comparison between two-dimensional and three-dimensional simulations was performed. It was found that, although 2D simulations are still useful, they overestimate the lifting process and therefore a 3D model is preferable. The influence of the magnitude of the restitution and friction coefficients on the process was also studied.

1. Introduction

The importance of dust lifting behind shock waves is due to applications in chemical and physical engineering, in process technology and safety. Within the field of process safety, layers of organic or inorganic dust can be entrained when an intentional or accidental pressure wave is produced in, for instance, coal mines or chemical processing units. As a consequence, the created dust cloud combined with other substances, which may be present in the environment, can form a dangerous, ignitable mixture that can be easily ignited. This type of phenomenon describes, for example, dust explosions in coal mines. This is the reason behind the fact that dust lifting processes have been the subject of numerous research efforts during the recent years. Experimental studies (e.g. Fletcher, 1976; Kauffman et al., 1992; Klemens et al., 2006; Lebecki et al., 1995) were performed to determine the mechanisms responsible for the entrainment of dust and creation of a particle cloud behind shock waves. It is fair to say that this kind of experiments are costly, difficult to reproduce and require very accurate measurement apparatus in order to obtain useful data. It is therefore difficult to find specific and reliable data for model validation.

Numerical simulations of the process were performed using two distinctive techniques: the Eulerian–Eulerian and the Eulerian–Lagrangian techniques. The former method is described and assessed in numerous studies (e.g. Igra et al., 2004; Kosinski et al., 2005; Mathiesen et al., 2000; Rogue et al., 1998; Samuelsberg and Hjertager, 1996; Thevand and Daniel, 2002) and is considered a good engineering tool as both the fluid and solid phase are considered as inter-penetrating continua. The latter is considered a better phenomenological tool to study the fundamental processes of dust lifting (Chang and Kailasanath, 2003; Kosinski and Hoffmann, 2005; Kosinski et al., 2005; Lu et al., 2005) since each solid particle is traced in the simulation domain. It was found that the collisions that take place between the solid particles and their surroundings (walls or other particles), along with considering two-way coupling, represent important factors governing the process of dust lifting (Kosinski and Hoffmann, 2005; Kosinski et al., 2005).

So far, the majority of the research studies on dust lifting have only described processes in two-dimensional domains. This was done mostly due to computation limitations. Even considering a medium size 3D simulation domain or tracking a large number of particles has been computationally problematic until recently. Results of 2D simulations have been useful both in engineering applications and in fundamental studies, but not all mechanisms of the process have been fully understood. Some of these shortcomings can be addressed and possibly solved using a three-dimensional model as it is closer to a real-life scenario. Such simulations are time-consuming, due to the very high number of computations, but it is becoming a very useful tool to study the phenomena behind dust lifting.

The aim of this paper is to model a dust lifting process in a three-dimensional domain using the Eulerian–Lagrangian modelling technique. Emphasis was put on the importance of considering

* Corresponding author.
E-mail address: catalin.ilea@ift.uib.no (C.G. Ilea).

0301-9322/$ - see front matter © 2008 Elsevier Ltd. All rights reserved.
doi:10.1016/j.ijmultiphaseflow.2008.02.007

particle collisions. For this, simulations were run with a varying number of particles in the layer and statistical parameters have been studied. Also, possible improvements to the model were sought in order to improve its accuracy and efficiency. Due to the lack of reliable literature data on the process it is difficult to produce a validation of the model. One of the main problems of experimental studies is the inability of tracking particle trajectories accurately. In spite of these limitations, some qualitative comparisons with previous experimental and numerical studies are presented. The influence of collision parameters on some statistical results of the simulations was also assessed.

2. The mathematical model

The mathematical model needs to incorporate the mathematical expressions that govern the flow of the gas, the motion of the particles and the interphase interactions that occur in a dust lifting process. In this paper the Eulerian–Lagrangian modelling technique was employed. This means that the gas phase behaviour was modelled in a Eulerian frame of reference and the motion of the solid phase was resolved in a Lagrangian frame of reference.

2.1. Equations for the gas phase

Because the modelled gas flow is a shock wave, it suffices to solve the Euler equations rather than the full equations of motion. The Euler equations were modified in order to account for interphase interactions. Therefore, these may be written as

$$\frac{\partial \rho}{\partial t} + \nabla \cdot (\rho \vec{u}) = 0 \quad \text{conservation of mass}, \tag{1}$$

$$\frac{\partial \rho \vec{u}}{\partial t} + \nabla \cdot ((\rho \vec{u}) \otimes \vec{u}) + \nabla p = S_{\mathrm{I}} \quad \text{conservation of momentum}, \tag{2}$$

$$\frac{\partial E}{\partial t} + \nabla \cdot (\vec{u}(E+p)) = S_{\mathrm{II}} \quad \text{conservation of energy}. \tag{3}$$

In these equations, the time and space dependent variables are: the gas pressure p, the gas density ρ, the gas velocity $\vec{u}$ and the total energy of the gas per unit volume E. The source term S_{I} represents the action of the particles on unit volume of gas and it can be written as

$$S_{\mathrm{I}} = -\sum_{i}^{N_{\mathrm{p}}} \vec{f}_{\mathrm{p},i}, \tag{4}$$

where N_{p} is the number of particles per unit volume and $\vec{f}_{\mathrm{p},i}$ is the force acting on particle i. Similarly, the energy source term S_{II} is

$$S_{\mathrm{II}} = -\sum_{i}^{N_{\mathrm{p}}} \vec{f}_{\mathrm{p},i} \cdot \vec{v}_i, \tag{5}$$

where $\vec{v}_i$ is the velocity of particle i.

Because there are fewer equations than variables, it is necessary to add one more equation, the gas equation of state:

$$p = \rho \cdot R_{\mathrm{g}} \cdot T, \tag{6}$$

where R_{g} represents the specific gas constant and T is its temperature. The gas temperature and gas energy are linked through the following equation:

$$E = \frac{\rho \cdot R_{\mathrm{g}} \cdot T}{\gamma - 1} + \frac{\rho u^2}{2}, \tag{7}$$

where γ is the adiabatic index of the gas.

2.2. Equations for the solid phase

The motion of each particle is modelled individually by applying Newton's second law of motion,

$$m_i \frac{\mathrm{d}\vec{v}_i}{\mathrm{d}t} = \vec{f}_{\mathrm{p},i}. \tag{8}$$

Here, the specific variables for particle i are: m_i particle mass; $\vec{v}_i$ particle velocity. The particles are moving under the influence of the drag force, which acts upon them due to the gas movement relative to them. At high Reynolds numbers, this force has a dominant role over other forces (Crowe et al., 1998). Previous studies, e.g. Zydak and Klemens (2007), have mentioned that implementing lift forces has very little or no effect on the model predictions. Therefore, only the drag force is considered in this model and is computed as

$$\vec{f}_{\mathrm{p},i} = C_{\mathrm{D}} A_{\mathrm{p}} \rho \frac{|\vec{u} - \vec{v}_i|(\vec{u} - \vec{v}_i)}{2}, \tag{9}$$

where C_{D} is the drag force coefficient and A_{p} represents the projected area of the particle on a plane normal to the direction of motion. This drag law enables the consideration of viscous effects due to the presence of the particle. The momentum exchange between the wall and the gas phase will be mediated by the particles in the vicinity of the dust layer. Particle–wall, inter–particle and fluid–particle interactions are responsible for this. In this particular type of process, the boundary layer is thin enough to be neglected. Neglecting boundary layer effects can be thus regarded as a minor error. The drag force coefficient C_{D} is a function of the relative Reynolds number, defined as

$$Re_{\mathrm{r}} = \frac{\rho d_i |\vec{u} - \vec{v}_i|}{\mu} \tag{10}$$

where d_i represents the particle diameter, μ is the gas viscosity.

The empirical formula of Clift and Gauvin (1970) was used to compute the drag coefficient

$$\frac{C_{\mathrm{D}} Re_{\mathrm{r}}}{24} = 1 + 0.15 Re_{\mathrm{r}}^{0.687} + 0.0175 Re_{\mathrm{r}} (1 + 4.25 \cdot 10^4 Re_{\mathrm{r}}^{-1.16})^{-1} \tag{11}$$

Due to possible high velocity differences between gas and particles, the latter might be subjected to some compressibility effects. Therefore, the drag coefficient not only varies with the relative Reynolds number Re_{r}, but also with the relative Mach number M_{r}. According to Crowe et al. (1998), it is necessary to correct the value of C_{D} for this effect if $M_{\mathrm{r}} > 0.6$. We used their proposed empirical correction:

$$C_{\mathrm{D,c}} = 2 + (C_{\mathrm{D}} - 2)\mathrm{e}^{-3.07\sqrt{\gamma} G M_{\mathrm{r}}/Re_{\mathrm{r}}} + \frac{H}{\sqrt{\gamma} M_{\mathrm{r}}} \mathrm{e}^{-\frac{Re_{\mathrm{r}}}{2M_{\mathrm{r}}}}$$

with

$$G(Re_{\mathrm{r}}) = \frac{1 + Re_{\mathrm{r}}(12.278 + 0.548 Re_{\mathrm{r}})}{1 + 11.278 Re_{\mathrm{r}}} \tag{12}$$

$$H(M_{\mathrm{r}}) = \frac{5.6}{1 + M_{\mathrm{r}}} + 1.7\sqrt{\frac{T_{\mathrm{d}}}{T_{\mathrm{c}}}},$$

where T_{d} and T_{c} are the temperatures of the particles and the gas, respectively.

The change of the particle angular velocity due to the influence of the fluid phase is not considered in this model. However, the model considers particle rotation as a consequence of particle collisions.

2.3. Collision model

The hard-sphere model of Crowe et al. (1998) was used to model particle–wall and particle–particle collisions. In this approach, there are three basic assumptions:

(1) The deformation of the particles is neglected, therefore the distance between the centres of the spherical particles is the sum of the two particle radii.

(2) The particles slide along each other according to Coulomb's friction law.
(3) Once the particles stop sliding during a collision, they will roll over each other for the remainder of the collision and not resume sliding later.

The impulse equations must be solved in order to determine the emergent velocity and rotation of the particles. Crowe et al. (1998) give two sets of solutions for this problem, depending on whether the sliding stops (their case *a*) or not (their case *b*) during the collision process. We denote e as the coefficient of restitution for the collision and f as the Coulombic dynamic coefficient of friction. The coefficient of restitution is very important to the behaviour of the particles and can vary between 0 (for non-elastic collision) and 1 (for fully elastic collisions). The Coulombic friction coefficient is also significant when accounting for inter-particle and particle–wall collisions. The values of both coefficients are specified as constants in the model.

We now calculate the loss of mechanical energy with the aid of the exact model equations given in Crowe et al. (1998). Let $\vec{n}$ be the unit normal vector to the plane of collision and $\vec{G}^0$ the initial relative velocity vector of the particle pair defined as $\vec{G}^0 = \vec{v}_1^0 - \vec{v}_2^0$ where $\vec{v}_1^0$ and $\vec{v}_2^0$ are the initial translational velocities of the particles. Also, let $\vec{G}_{ct}^0$ be the initial tangential component of the relative velocity of the contact point and $\vec{t}$ the unit vector in the tangential direction. Considering that the particles are identical, with mass m and radius r, and that the total translational mechanical energy of a particle is $\frac{1}{2}m\vec{v}^2$, the loss of translational energy due to inter-particle collision is

$$E_{t,lost} = \frac{m}{2}((\vec{v}_1^0)^2 + (\vec{v}_2^0)^2 - \vec{v}_1^2 - \vec{v}_2^2). \tag{13}$$

Using the model equations for case *a*, this gives:

$$E_{t,lost} = \frac{m}{2}\vec{G}^0 \cdot (1+e)(\vec{n}\cdot\vec{G}^0)(\vec{n}+f\vec{t}) - \frac{m}{4}[(1+e)(\vec{n}\cdot\vec{G}^0)(\vec{n}+f\vec{t})]^2, \tag{14}$$

and for case *b* one obtains:

$$E_{t,lost} = \frac{m}{2}\vec{G}^0 \cdot \left\{\vec{n}(\vec{n}\cdot\vec{G}^0)(1+e) + \frac{2}{7}|\vec{G}_{ct}^0|\vec{t}\right\} - \frac{m}{4}\left\{\vec{n}(\vec{n}\cdot\vec{G}^0)(1+e) + \frac{2}{7}|\vec{G}_{ct}^0|\vec{t}\right\}^2. \tag{15}$$

The rotational mechanical energy of a particle is $\frac{1}{2}I\vec{\omega}^2$, where I is the particle moment of inertia and $\vec{\omega}$ is the rotation vector. For a spherical particle $I = \frac{2}{5}mr^2$. The loss of rotational mechanical energy during an inter-particle collision is

$$E_{r,lost} = \frac{1}{2}I((\vec{\omega}_1^0)^2 + (\vec{\omega}_2^0)^2 - \vec{\omega}_1^2 - \vec{\omega}_2^2), \tag{16}$$

where the index 0 denotes initial values.

Using the rotation vector solutions for case *a*, this becomes:

$$E_{r,lost} = \frac{mr}{2}(\vec{n}\cdot\vec{G}^0)(1+e)f(\vec{n}\times\vec{t})\cdot(\vec{\omega}_1^0 + \vec{\omega}_2^0) - \frac{5m}{8}[(\vec{n}\cdot\vec{G}^0)(1+e)f(\vec{n}\times\vec{t})]^2. \tag{17}$$

And finally, using the solutions for case *b*, the lost rotational energy is

$$E_{r,lost} = \frac{mr}{7}|\vec{G}_{ct}^0|(\vec{n}\times\vec{t})\cdot(\vec{\omega}_1^0 + \vec{\omega}_2^0) - \frac{5m}{98}[|\vec{G}_{ct}^0|(\vec{n}\times\vec{t})]^2. \tag{18}$$

The total loss of mechanical energy is $E_{t,lost} + E_{r,lost}$.

The collisions between a particle and a hard wall follow the same principles and they are dealt with in a similar manner. More details about the post-collisional velocity and rotation vectors can be found in Crowe et al. (1998).

2.4. Numerical techniques

A second-order flux corrected transport algorithm (LCPFCT) was implemented to solve the Euler equations given a sharp shock initial condition (Boris et al., 1993). The same method has been previously employed in studies of shock waves interacting with particles and droplets (Chang and Kailasanath, 2003).

In the Lagrangian approach, the particles are treated as point-like objects. Their behaviour is modelled in accordance with the forces that act upon them. Therefore, the positions of each particle and their velocities are calculated every time-step. The numerical scheme concerning the particle flow is

$$m_i\frac{\vec{v}_i^{n+1} - \vec{v}_i^n}{\Delta t} = C_D A_p \rho \frac{(\vec{u}^{n+1} - \vec{v}_i^{n+1})|\vec{u}^n - \vec{v}_i^n|}{2}, \tag{19}$$

$$x_i^{n+1} = x_i^n + \Delta t\frac{(v_{x,i}^{n+1} + v_{x,i}^n)}{2}, \tag{20}$$

$$y_i^{n+1} = y_i^n + \Delta t\frac{(v_{y,i}^{n+1} + v_{y,i}^n)}{2}, \tag{21}$$

$$z_i^{n+1} = z_i^n + \Delta t\frac{(v_{z,i}^{n+1} + v_{z,i}^n)}{2}. \tag{22}$$

The index i identifies each particle, n is the time-step index, x, y and z represent the components of the position vector, while v_x, v_y and v_z represent the components of the particle velocity vector.

The values of the gas velocity and gas energy are altered for each computational cell in accordance with the presence of particles, their volume fraction and the force acting upon them. This was done in order to account for two-way coupling.

2.5. Collision handling

An event-driven algorithm (Sundaram and Collins, 1996) was adopted in order to properly account for collisions. Its purpose is to detect the exact time of each collision within a time-step in order for all of them to be treated sequentially. The steps followed by the algorithm are presented in Fig. 1. At the beginning of each time-step the particles variables are advanced to the end of the full time-step. Next, the particles are checked for overlaps, i.e. if the distance between two particles is less than the sum of two particle radii or the distance between one particle and a wall is less than one particle radius. If this is the case, then a collision has to be handled within the time elapsed and the exact instant of collision has to be calculated. In order to achieve this, we assume that the particles are advancing with a constant speed within the time-step, equal to the average between the initial and final speed. The quadratic equation:

$$|\vec{r_{ij}} + \Delta t_{ij}^c \cdot \vec{G}_{ij}^0| = 2\cdot r \tag{23}$$

was solved to determine the time of collision for the particle pair *i*–*j*. The initial relative distance vector between particles is $\vec{r_{ij}}$ and r is the particle radius. Eq. (23) cannot be solved only along one of the axes, to make it linear, because the length of the axis component of the allowed distance between the particles cannot be determined. Since the equation is quadratic, one obtains two solutions for the time of collision Δt_{ij}^c. The smaller positive value represents the time necessary for the particles to achieve surface contact and the bigger positive value represents the time until the particles have completely passed through each other. Thus, the first solution is the one of interest and it is chosen to be compared with values calculated for other particle pairs in order to check for the minimum value of collision time. This is done in order to finally obtain the instant in time for the first collision.

The linear equation:

$$d_{i,w} + \Delta t_{iw}^c \cdot \vec{v}_i = 0 \tag{24}$$

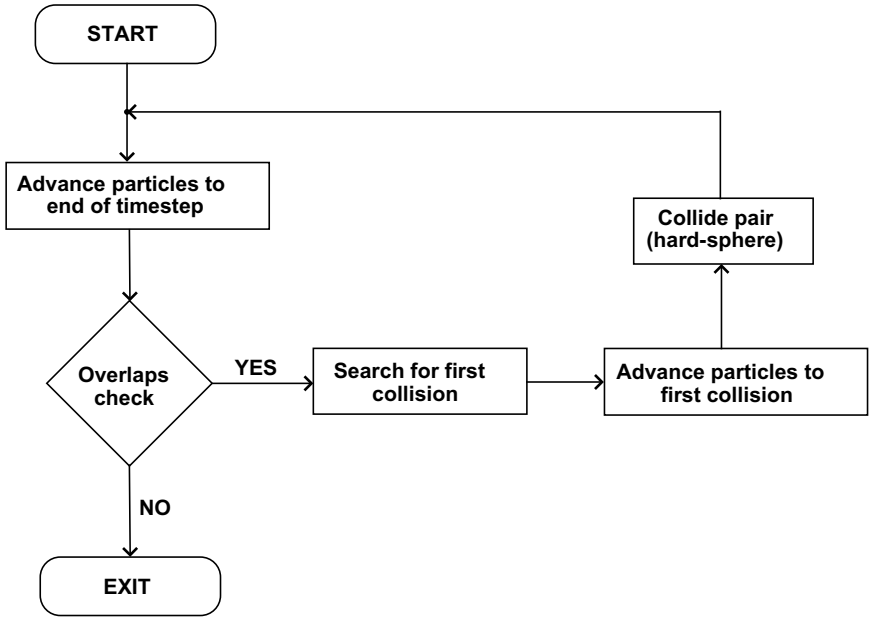

Fig. 1. The event-driven algorithm.

was solved when a particle–wall collision had to be handled. Here, $d_{i,w}$ represents the initial distance from particle i to the wall, $\vec{v}_i$ represents the average velocity of particle i (taken constant for this time interval) and Δt^c_{iw} is the unknown time of particle–wall collision.

It is important to mention that the overlap check can be done for each possible pair of particle. But, in this way a very long computation time is needed. This can be adjusted by using the so-called neighbour lists (Sundaram and Collins, 1996). A list of neighbours is created for each particle by setting a certain maximum vicinity distance. So, possible collisions are tested only among these. These neighbour lists must be updated after a number of time-steps have been passed. If a large update period is used, the computation time is significantly reduced, but this comes at the cost of possibly missing some collisions. On the other hand, a small value will only slightly decrease the computation time. Therefore, an appropriate value must be chosen. After successive trials, a value of 50 time-steps between updates was employed for this study.

After the exact time of the first collision is determined, all the particles are advanced to their position at this time. This is set as the new initial position. Next, the actual collision is handled using the hard-sphere model to calculate the post-collisional values of the particle translational and angular velocities.

In the end, the sequential steps are run again starting with the new initial position of the particles. The algorithm will run until the overlap check will give a negative result. It will start again in the next time-step.

3. Results and discussion

3.1. The dust lifting simulation parameters

For simulation purposes, a three-dimensional simulation domain was considered. The dimensions of the domain are 30 cm×1 cm×0.3 cm. In all simulations, the chosen grid was uniform along all axes. The computational cell was represented by a cube and had a side length of 0.25 mm. The LCPFCT algorithm was tested for grid sensitivity.

At the boundary, the fluid density, pressure and tangential velocity components were set the same values as in the first/last cell of the actual domain, respectively. Mirror boundary conditions were employed for the fluid velocity component that is normal to the boundary. Ambient air parameters were used for the fluid phase physical properties. In order to generate a shock wave, the domain was initially split into two regions, a high pressure region and a low pressure one. An imaginary membrane was placed parallel to the y–z plane at 2 cm along the x-axis to separate the two sections. Thus, the high pressure section is 1/15 of the total channel volume. However, the left boundary condition of this chamber is such that high pressure gas is supplied freely as gas exits the chamber to the right during the simulation. A pressure difference of 4 bar was set for all dust lifting simulations. The initial temperature was set identical in both regions at 20 °C. When the membrane was removed, a shock wave started to propagate at a Mach number of 1.33. Thus, a steady shock wave is obtained.

A set of different simulations was done considering an increasing number of particles (5000, 7000 and 9000). This increase only affected the thickness of the initial particle layer, its width and length were kept constant. The initial layer extends only a few rows of cells in the z direction; the cell size cannot be made smaller lest the particle size becomes comparable to the cell size. However, as the simulation starts, the particles will quickly spread over a larger number of cells. All of the particles were considered spherical and identical with a 100 μm diameter. Coal dust normally has a density in the range 1000–1500 kg/m^3, and for this reason a particle density of 1000 kg/m^3 was chosen for these simulations. The particle layer was initially placed immediately in front of the shock wave, in regular arrays. Their positions were then altered by a small random value in order to obtain a random initial placement of particles in a compact layer. An example of such a particle placement is given in Fig. 2. The volume fraction of the particles in the initial layer is 9.5%. With this initial position the dust layer will primarily interact with a mixture of driver and driven gas. This does not cause problems since neither temperature effects nor chemical reactions are studied at this stage.

Concerning the collision hard-sphere model, the value of Coulomb's friction coefficient was set at 0.15 and the restitution coefficient was 0.8 in accordance with suggestions from Goldschmidt et al. (2001).

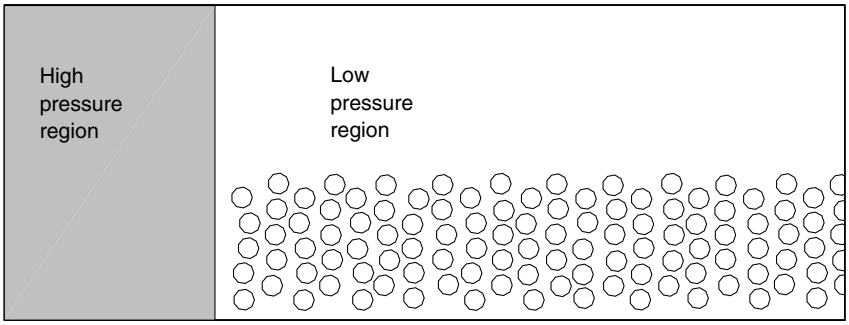

Fig. 2. Example of particle placement.

3.2. Simulations with varying number of particles

Different simulations were performed for each initial layer thickness. Fig. 3 shows the time evolution of the dust lifting process of 5000 particles, in the x–z plane. Fig. 4 presents a closer look at the front of the particle layer, after 1.2 ms. It can be observed that, due to the passage of the shock wave, particles are moved both in the direction of the wave and normal to it. Particles are blown forward for a certain distance but due to them shielding each other from the effects of the gas flow, the effect is rather moderate as opposed to one-way coupling simulations. This shielding effect is particularly clear in the early snapshots, where particles are seen to be blown off the front of the particle layer by the passing shock wave, while the particles within the layer are much less affected.

The dust layer snapshots presented in Figs. 3 and 4 show profiles that are qualitatively similar to the experimental ones presented by Gerrard (1963) or two-dimensional numerical ones by Kosinski and Hoffmann (2005).

In order to make a statistical study of the process a few parameters such as average height of particles, mean squared displacement of particles and cumulative number of collisions have been compared. The average height as a function of time was calculated as:

$$h(t) = \frac{1}{N}\sum_{i=1}^{N} z_i(t), \tag{25}$$

where N represents the total number of particles and z_i represents the elevation of particle i. The evolution of the average height for each simulation is presented in Fig. 6.

To calculate the mean squared displacement of the particles as a function of time, the following equation was used:

$$\mathrm{MSD}(t) = \frac{1}{N}\sum_{i=1}^{N}[(x_i(t) - x_{i,0})^2 + (y_i(t) - y_{i,0})^2 + (z_i(t) - z_{i,0})^2]. \tag{26}$$

Here, $x_{i,0}$, $y_{i,0}$ and $z_{i,0}$ represent the initial coordinates of particle i. The particle displacement chart is shown in Fig. 7. Fig. 8 presents the cumulative number of collisions versus time. This parameter has been also chosen as a worst-case in terms of the reproducibility of the simulations, since it presented the largest spread of results during repeated simulations. Fig. 9 presents results from three repeat simulations and it can be noticed that they are reproducible as they render similar statistical results.

Lifting of the particles is mainly due to particle–wall and particle–particle collisions. Fig. 8 shows, not surprisingly, that the cumulative number of collisions is higher in the simulations with the higher number of particles, by the end of the simulated timeframe. It can also be seen that the cumulative number of collision is higher for 5000 particles and lower for the other two cases, during much of the first half of the simulation. However, the rate of increase in number of collisions (the slopes of the curves) starts to decrease significantly for 5000 particles, while for the other two cases it does not. This difference seems to be the result of two

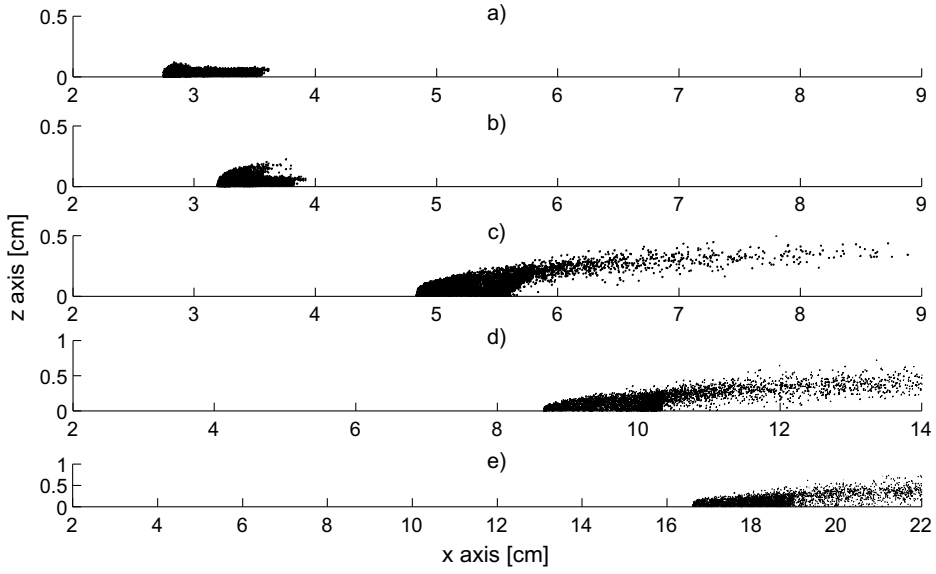

Fig. 3. Particle positions in the channel after: (a) 0.4 ms; (b) 0.6 ms; (c) 1.2 ms; (d) 2 ms; (e) 3 ms. Simulation of 5000 particles.

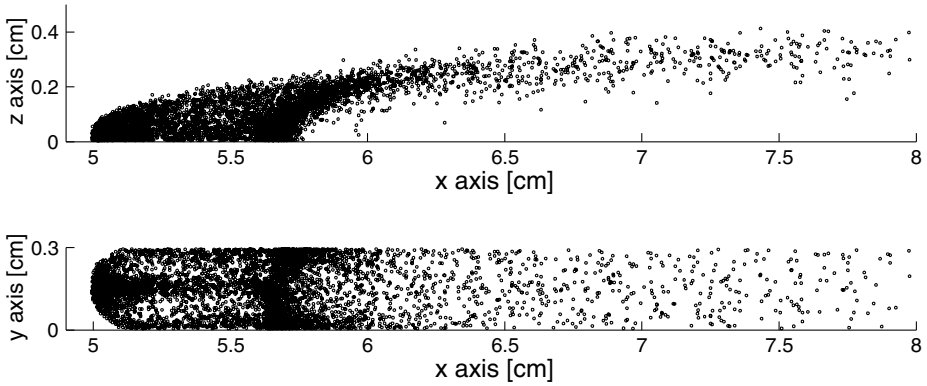

Fig. 4. Front of particle layer at 1.2 ms. Simulation of 5000 particles.

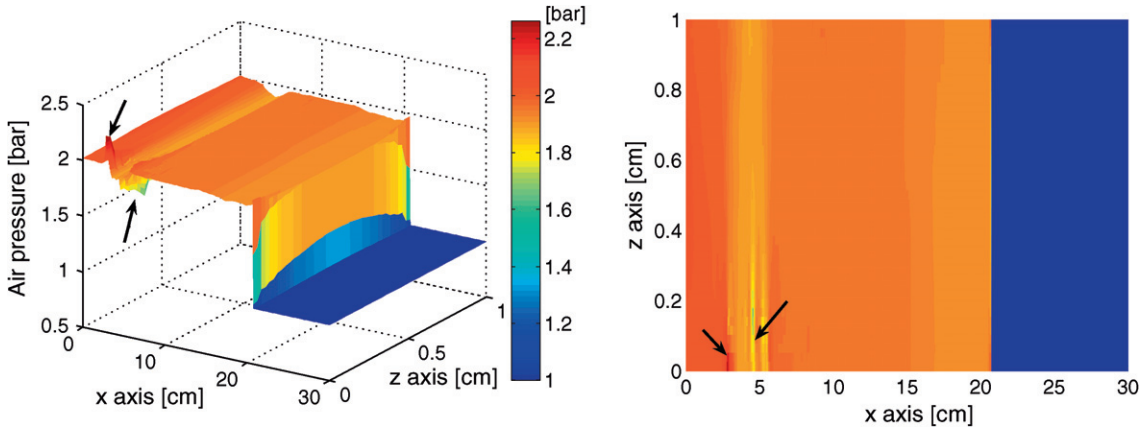

Fig. 5. Air pressure profile in an x–z plane after 0.4 ms of simulated time.

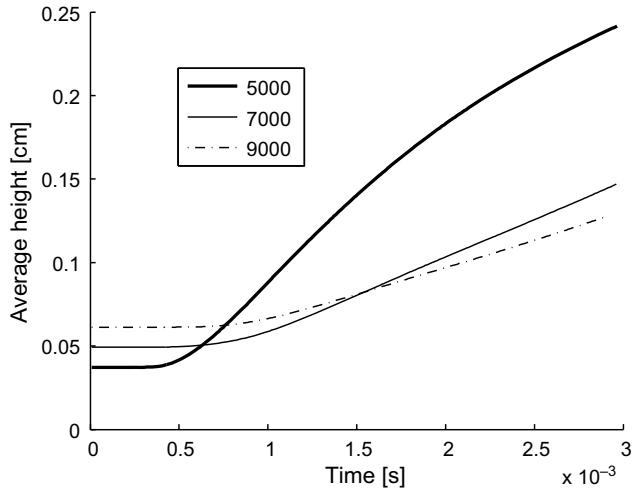

Fig. 6. Average height of particles as a function of time.

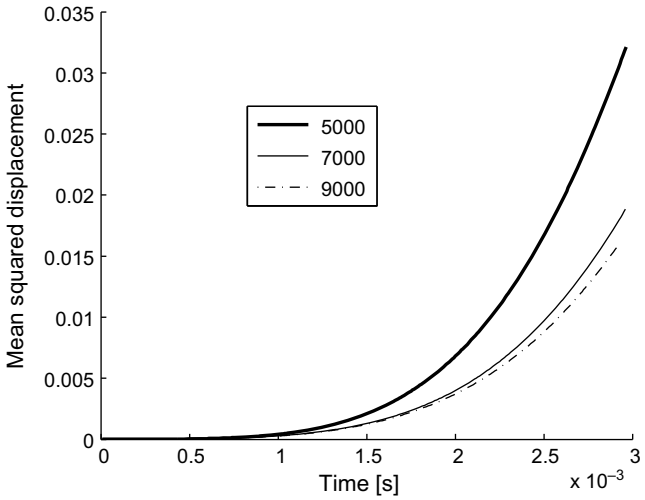

Fig. 7. Mean squared displacement of particles as a function of time.

opposing effects. On one hand, having more particles with similar mobility increases the frequency of particle collisions. On the other hand, the shielding effect, which is stronger in the cases involving more particles, acts to decrease the individual particle mobility caused by the shock wave. Fig. 6 furthermore shows that the lifting of the particles, within the time-frame simulated, is more significant than the fewer the particles.

The over-all impression is thus that the fewer the particles in the layer, the larger the particle mobility and the more efficient the effect of collisions in bringing about particle lift. As the inter-particle spacing increases due to the lifting, the rate of increase in the cumulative collision number decreases. This latter feature is probably reflected in the slight decrease in the rate of particle rise for the case of 5000 particles seen in Fig. 6, towards the end

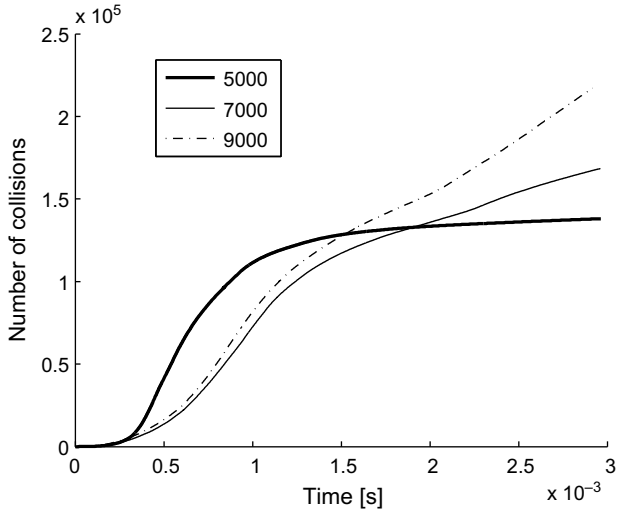

Fig. 8. Cumulative number of collisions as a function of time.

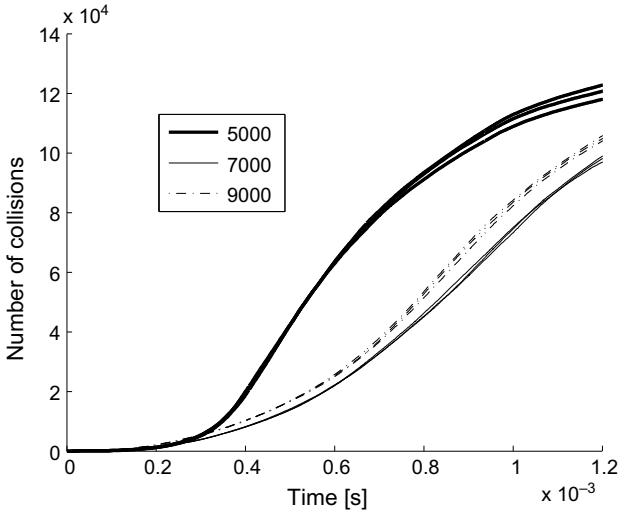

Fig. 9. Reproducibility of simulations.

of the simulation. Consistent with this it is seen in Fig. 7 that the mean squared displacement is higher for the case of 5000 particles than for the two other cases. All the trends with number of particles in the layer seen in Figs. 6–8 can be attributed to the varying influence of the "shielding" effect. This underscores the importance of taking into account two-way coupling in this type of simulation. To illustrate this, from the point of view of the fluid phase, Fig. 5 presents the pressure profile of air in an x–z plane situated in the middle of the channel. It can be observed that the presence of the particles has created specific structures in the pressure profile. A high pressure region can be observed in front of the particle layer, while behind them there is a low pressure region.

Another important factor that may influence the statistics of the process is the surface roughness of the walls. In a previous study by Ilea et al. (2007) it was found that wall roughness did influence simulation results in two-dimensional domains. However, a roughness model for the present three-dimensional simulations has not been developed.

In order to have an account of the particle energy change, the averaged kinetic energy evolutions of the particles along each of the axes (the forward direction x, the lateral direction y and the upward direction z) are presented in Figs. 10–12, respectively. The level of the kinetic energy is also a good indicator of the entrainment process.

It can be seen that the fewer the particles the more translational energy they possess. This is natural since the shock wave energy is the same in all simulations and some of it is transferred to an increasing number of particles. Since the shielding effect seems to have been overcome to a significantly larger extent in the 5000 particles case, there is a large difference in the amount of energy that the particles possess on average compared to the other two cases. However, as the collision process settles down, there is significant decrease of energy in the lateral and vertical directions, meaning that particles are mostly blown in the same direction as the gas. But the particle energy account is not complete if the loss of energy due to collisions is not considered. Fig. 13 presents a cumulative account of these losses. The effects observed in this chart are directly linked to Fig. 8. Having on average initially achieved a higher interparticle spacing during the simulation, the 5000 particles case has produced more collisions, efficient in terms of producing lifting, and an associated higher mechanical energy

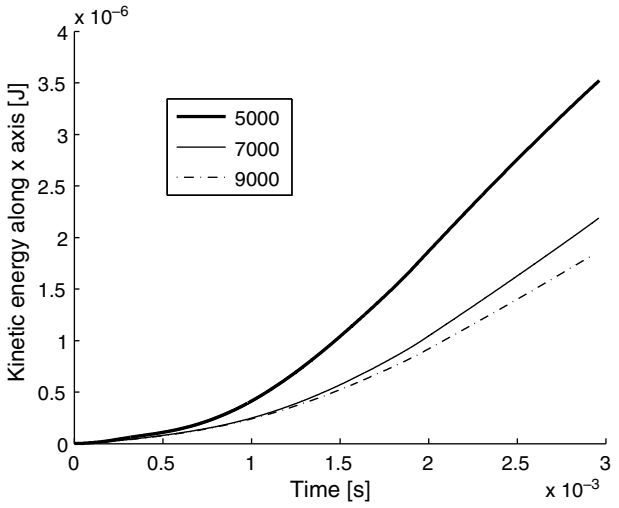

Fig. 10. Particle averaged kinetic energy of particles along the x-axis as a function of time.

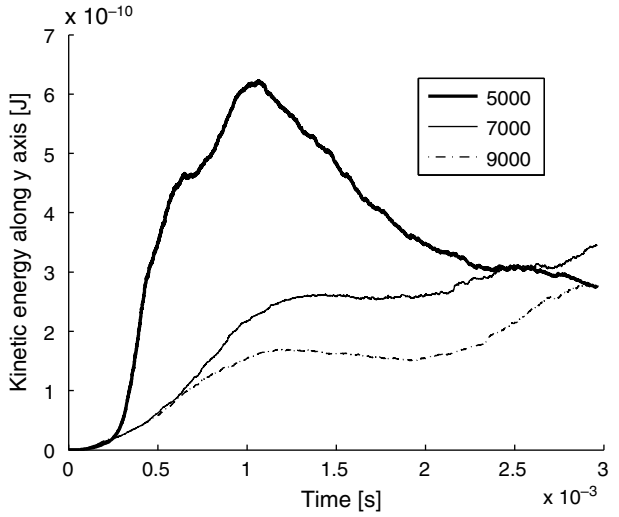

Fig. 11. Particle averaged kinetic energy of particles along the y-axis as a function of time.

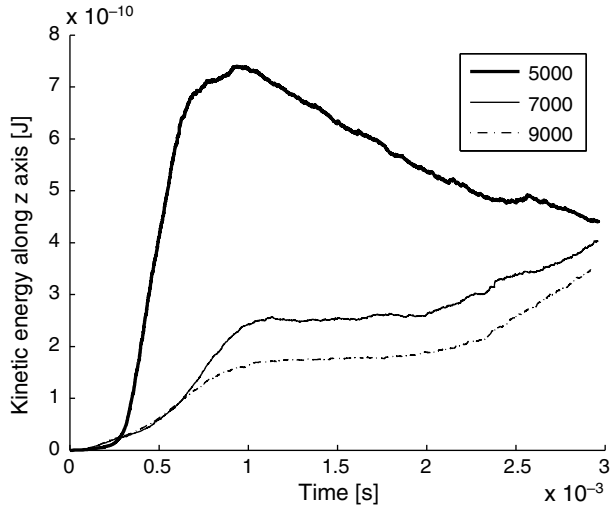

Fig. 12. Particle averaged kinetic energy of particles along the z-axis as a function of time.

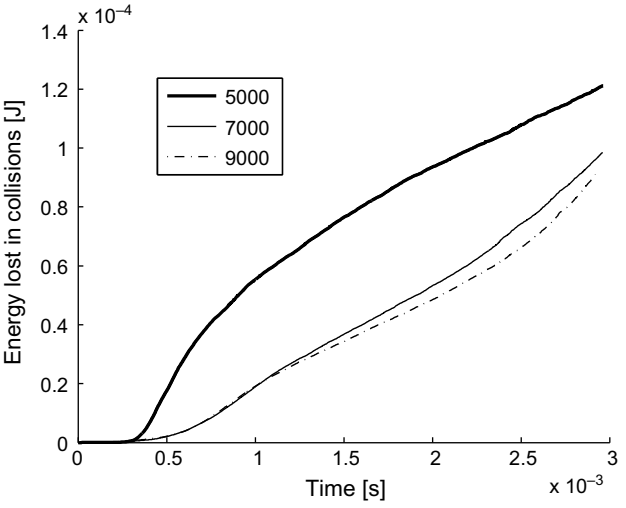

Fig. 13. Total lost energy by particles in collisions. Values are cumulated.

loss. As the number of collisions starts to decrease, so does the slope of the lost energy curve and conversely for the cases involving 7000 and 9000 particles. Therefore, it can be concluded that the average energy loss due to a collision is lower the more particles are involved in the simulation.

A comparison of the average particle height between two-dimensional and three-dimensional simulations of dust lifting is presented in Fig. 14. These results come from simulating particle layers of the same thickness and length. It may be observed that the 2D simulations overestimate the lifting process. This was to be expected since collisions result in only vertical transverse movement in the 2D case while they may also give rise to horizontal transverse movement in the 3D case. We note, on the other hand, that the two types of simulation agree globally.

Amending the particle collision model in a two-dimensional simulation to account for three-dimensional movement could improve the model, causing time-saving two-dimensional simulations to give more accurate results. This will require a stochastic model.

In order to determine the effect of the compressibility correction, the simulation of 5000 particles has been compared with

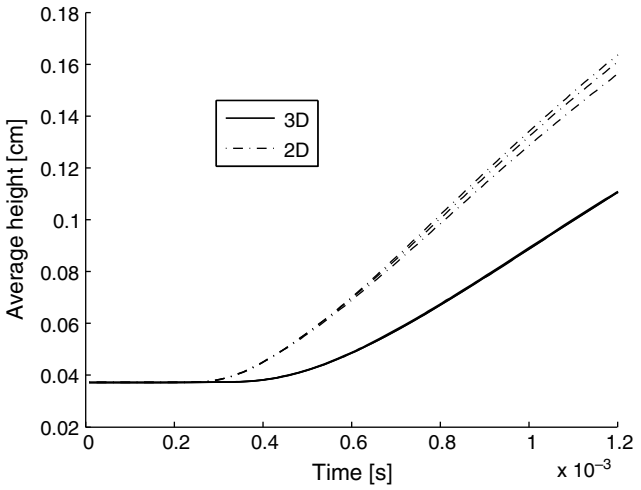

Fig. 14. Comparison of average heights of particles as a functions of time.

similar simulations but without including the compressibility correction in the model. Fig. 15 presents a comparison between their results. It may be observed that the model only slightly overestimates the average height of the particles if the compressibility correction is not included. An explanation might come from the fact that the threshold of $M_r > 0.6$ for applying the correction is only satisfied for a few of the particles.

3.3. Simulations with varying restitution and friction coefficients

The restitution and friction coefficients are two important parameters with regard to particle collisions. The statistics of the process depend on their value. The coefficient of restitution e is, somewhat surprisingly, not strongly material dependent, and is more related to the collision conditions (Goldschmidt et al., 2001; Yao et al., 2003). In contrast, the friction coefficient f can more appropriately be considered a material property, although process conditions (e.g. humidity) may have some influence on its value. The values for f of some materials range from low kinetic friction (e.g. coal–coal, 0.1–0.2) to high kinetic friction (e.g. glass–glass, 0.4–0.6).

Simulations have been performed in order to determine the influence of the restitution and friction coefficients on the statistical parameters of the dust lifting process. For this, the case of 5000

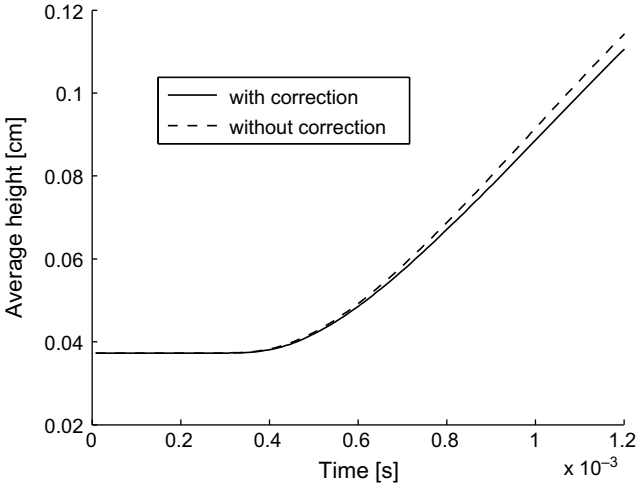

Fig. 15. Influence of the compressibility correction.

particles has been chosen. The chosen values for e and f are shown in Table 1. The base case is that of $(e,f) = (0.8, 0.15)$, and the values of e and f are each varied independently over three levels around this base case.

Fig. 16 shows the influence of e and f on the average particle height. It can be observed that the restitution coefficient has the more significant impact on these statistical results. Fully elastic collisions lead to a higher lifting effect, while more plastic collisions reduce the average height values of the particle layer. Fig. 17 shows the cumulative number of collisions for each simulation. Decreasing e for a constant value of f is seen to increase the number of collisions, at the lower level of e quite dramatically so. Increasing f, on the other hand, gives rise to a moderate increase in the number of collisions. However, the friction coefficient is much more influential when it comes to the lost energy during collisions. In Fig. 18, a greater value for f leads to high values of the total energy loss, while disregarding friction altogether ($f = 0$) leads to the lowest energy loss values. The energy loss in this latter case is caused by the mechanical energy dissipation due to the normal component of the impact only.

Table 1
Values of e and f

e	0.6	1.0	0.8	0.8	0.8
f	0.15	0.15	0.0	0.3	0.15

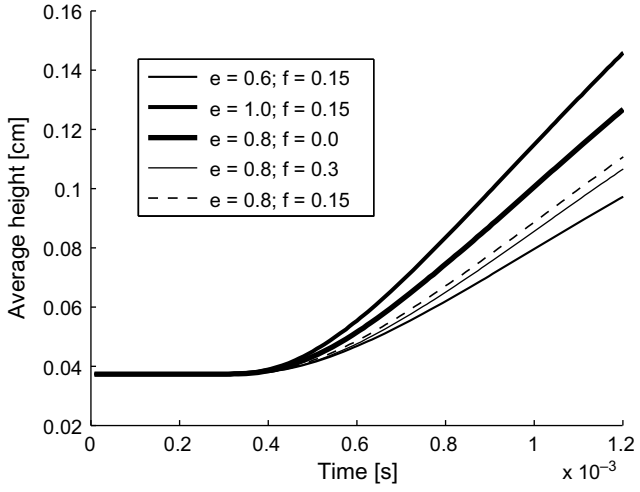

Fig. 16. Average height of particles as a function of time.

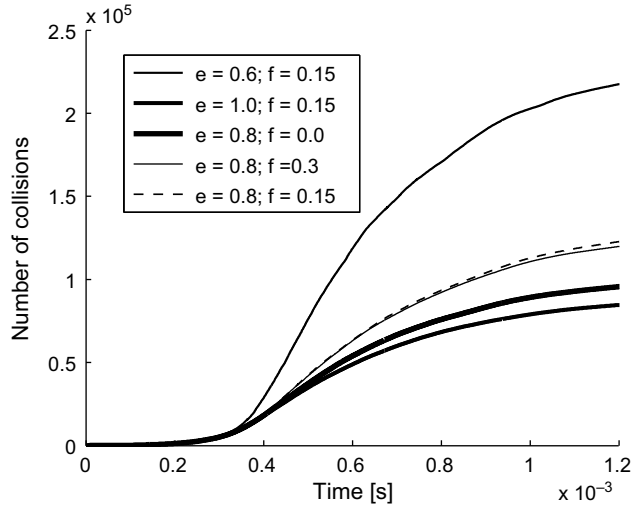

Fig. 17. Cumulative number of collisions as a function of time.

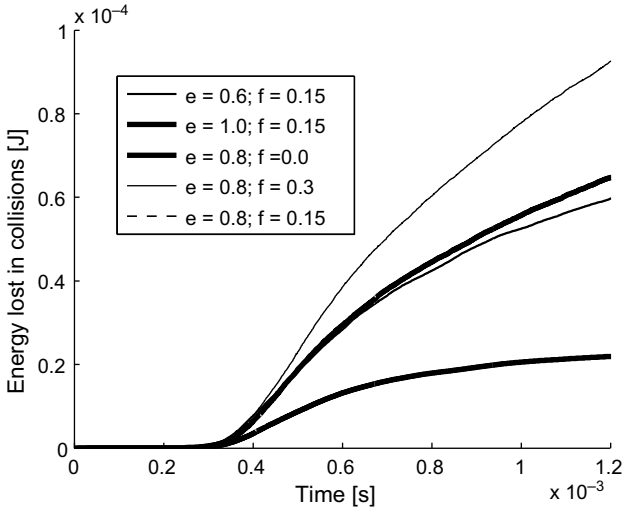

Fig. 18. Total lost energy by particles in collisions. Values are cumulated.

4. Concluding remarks

This research aimed at modelling a dust lifting process inside a 3D channel where a particle layer has been placed at the bottom. The Eulerian–Lagrangian modelling technique was adopted since it is the only way that particle interactions can be accounted for in fundamental manner and this is one of the main causes for the lifting process, even though the computational cost is higher when compared to the Eulerian–Eulerian technique. However, this disadvantage decreases in time as computer speeds are rising steadily. A particular emphasis was put on the study of the inter-particle collisions and the particle–wall collisions. Results have shown that collisions are of crucial importance to the development of the process of dust lifting behind a shock wave. Comparative simulations of different layer thicknesses have shown that as the layer thickness increases the lifting effect is less intense (see Fig. 6). More particles, having on average less energy are displaced less (see Fig. 7). Due to the effect of particle shielding, the individual particle mobility is lower and the number of collisions initially takes on lower values for the cases where more particles are simulated (see Fig. 8). Also in these cases the particles possess less translational energy (see Figs. 10–12). The situation reverses as the collision process starts to gain on the shielding effect. Also, comparing some of these results to similar two-dimensional simulations, it was found that the latter render higher lifting effects due to the lack of lateral particle movement in the 2D model. These results demonstrate that, although 2D simulations of dust lifting are still useful, a 3D model has to be considered in order to have quantitatively accurate results (see Fig. 14). It was also shown that compressibility effects, due to high relative velocities between the fluid and the solid phase, have a slight influence on the lifting effect producing marginally lower values of the average height of particles (see Fig. 15). This type of model can also be extended and modified to simulate various other particle transport processes.

This work also presented results showing the influence of the collision parameters (the coefficient of restitution e and the friction coefficient f) on the statistical results of the simulations. It was found that the restitution coefficient is more influential when

accounting for the average height of particles (see Fig. 16) and the cumulative number of collisions (see Fig. 17) while the friction coefficient has, as expected, a significant influence on the total loss of energy during particle collisions (see Fig. 18).

Acknowledgements

The authors thank the Norwegian Research Council (NFR) for funding this research.

References

Boris, J.P., Landsberg, A.M., Oran, E.S., Gardner, J.H., 1993. LCPFCT – flux-corrected transport algorithm for solving generalized continuity equations. Naval Res. Lab.

Chang, E.J., Kailasanath, K., 2003. Shock wave interactions with particles and liquid fuel droplets. Shock Waves 12, 333–341.

Clift, R., Gauvin, W.H., 1970. The motion of particles in turbulent gas streams. In: Proc. Chemeca' 70, 1:14.

Crowe, C., Sommerfeld, M., Tsuji, Y., 1998. Multiphase Flows with Droplets and Particles. CRC Press LLC.

Fletcher, B., 1976. The interaction of a shock with a dust deposit. J. Phy. D: Appl. Phys. 9, 197–202.

Gerrard, J.H., 1963. An experimental investigation of the initial stages of the dispersion of dust by shock waves. British J. Appl. Phys. 14, 186–192.

Goldschmidt, M.J.V., Kuipers, J.A.M., van Swaaij, W.P.M., 2001. Hydrodynamic modelling of dense gas-fluidised beds using the kinetic theory of granular flow: effect of coefficient of restitution on bed dynamics. Chem. Eng. Sci. 56, 571–578.

Igra, O., Hu, G., Falcovitz, J., Wang, B.Y., 2004. Shock wave reflection from a wedge in a dusty gas. Int. J. Multiphas. Flow 30, 1139–1169.

Ilea, C.G., Kosinski, P., Hoffmann, A.C., 2007. Simulation of a dust lifting process in a two-dimensional domain with rough walls. In: Proceedings of PARTEC, Nuremberg, Germany, 2007.

Kauffman, C.W., Sichel, M., Wolanski, P., 1992. Research on dust explosions at the University of Michigan. Powder Technol. 71, 119–134.

Klemens, R., Zydak, P., Kaluzny, M., Litwin, D., Wolanski, P., 2006. Dynamics of dust dispersion from the layer behind the propagating shock wave. J. Loss Prevent. Proc. 19, 200–209.

Kosinski, P., Hoffmann, A.C., 2005. Modelling of dust lifting using the Lagrangian approach. Int. J. Multiphas. Flow 31, 1097–1115.

Kosinski, P., Hoffmann, A.C., Klemens, R., 2005. Dust lifting behind shockwaves: comparison of two modelling techniques. Chem. Eng. Sci. 60, 5219–5230.

Lebecki, K., Cybulski, K., Sliz, J., Dyduch, Z., Wolanski, P., 1995. Large scale grain dust explosions-research in Poland. Shock Waves 5, 109–114.

Lu, H., Wang, S., Zhao, Y., Yang, L., Gidaspow, D., Ding, J., 2005. Prediction of particle motion in a two-dimensional bubbling fluidized bed using discrete hard-sphere model. Chem. Eng. Sci. 60, 3217–3231.

Mathiesen, V., Solberg, T., Hjertager, B.H., 2000. An experimental and computational study of multiphase flow behaviour in a circulating fluidised bed. Int. J. Multiphas. Flow 26, 387–419.

Rogue, X., Rodriguez, G., Haas, J.F., Saurel, R., 1998. Experimental and numerical investigation of the shock-induced fluidization of a particles bed. Shock Waves 8, 29–45.

Samuelsberg, A., Hjertager, B.H., 1996. An experimental and numerical study of flow patterns in a circulating fluidized bed reactor. Int. J. Multiphas. Flow 22, 575–591.

Sundaram, S., Collins, L.R., 1996. Numerical considerations in simulating a turbulent suspension of finite-volume particles. J. Comp. Phys. 124, 337–350.

Thevand, N., Daniel, E., 2002. Numerical study of the lift force influence on two-phase shock tube boundary layer characteristics. Shock Waves 11, 279–288.

Yao, W., Chen, B., Liu, C., 2003. Energetic coefficient of restitution for planar impact in multi-rigid-body systems with friction. Int. J. Impact Eng. 31, 255–265.

Zydak, P., Klemens, R., 2007. Modelling of dust lifting process behind propagating shock wave. J. Loss Prevent. Proc. 20, 417–426.